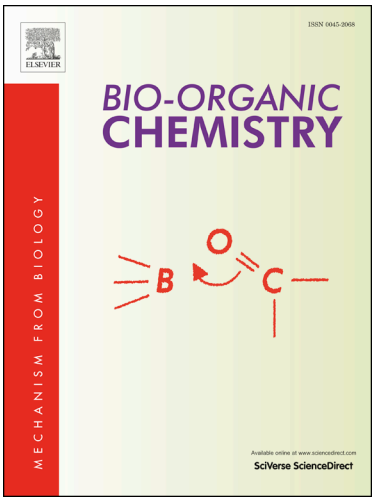

Design, synthesis and biological evaluation of 1,3-dihydroxyxanthone derivatives: Effective agents against acetylcholinesterase

Cintia A. Menéndez, Brunella Biscussi, Sebastián Accordino, A. Paula Murray, Darío C. Gerbino, Gustavo A. Appignanesi

PII: S0045-2068(17)30552-7
DOI: https://doi.org/10.1016/j.bioorg.2017.09.012
Reference: YBIOO 2132

To appear in: *Bioorganic Chemistry*

Received Date: 24 July 2017
Revised Date: 16 September 2017
Accepted Date: 18 September 2017

Please cite this article as: C.A. Menéndez, B. Biscussi, S. Accordino, A. Paula Murray, D.C. Gerbino, G.A. Appignanesi, Design, synthesis and biological evaluation of 1,3-dihydroxyxanthone derivatives: Effective agents against acetylcholinesterase, *Bioorganic Chemistry* (2017), doi: https://doi.org/10.1016/j.bioorg.2017.09.012

Design, synthesis and biological evaluation of 1,3-dihydroxyxanthone derivatives: Effective agents against acetylcholinesterase

Cintia A. Menéndez, Brunella Biscussi, Sebastián Accordino, A. Paula Murray, Darío C. Gerbino*, Gustavo A. Appignanesi

INQUISUR, Departamento de Química, Universidad Nacional del Sur (UNS)-CONICET, Avenida Alem 1253, 8000 Bahía Blanca, Argentina.

* **Corresponding author**. E-mail address: dgerbino@uns.edu.ar (D. C. Gerbino). Tel./fax: +54 (0) 291 459 5187.

Abstract: The present work concerns the rational design and development of new inhibitors of acetylcholinesterase (AChE) based on the privileged xanthone scaffold. In order to understand and rationalize the mode of action of these target structures a theoretical study was initially conducted. From the results of rational design, a new variety of amphiphilic xanthone derivatives were synthesized, structurally characterized and evaluated as potential anti-Alzheimer agents. The results showed that most of the synthesized compounds exhibited high AChE inhibitory activity at the micromolar range (IC_{50}, 0.46–12.09 μM). The synthetic xanthone **11** showed the best inhibitory effect on AChE and a molecular modeling study revealed that **11** targeted both the catalytic active site (CAS) and the peripheral anionic site (PAS) of AChE. Therefore, this compound could be considered as a potential lead compound towards new drugs for the treatment of Alzheimer's disease.

Keywords: Rational design; Synthesis; Amphiphilic xanthones; Acetylcholinesterase inhibitors; Molecular simulation.

1. Introduction

Alzheimer's disease (AD) is a neurodegenerative disorder that results in the progressive and irreversible cognitive impairment, memory loss, and decline in language.[1] Several factors, both genetic and environmental, have been considered to play a crucial role in its pathogenesis:

progressive loss of cholinergic neural transmission, formation of a beta-amyloid plaques (Aβ-plaques) that produces senile plaques (SPs) and neurofibrillary tangles (NFTs) of hyperphosphorylated tau protein.[2,3]

The current standard of care for mild to moderate AD, based on the so-called cholinergic hypothesis, includes treatment with AChE inhibitors (AChEI) to improve cognitive function.[4,5] Some examples of drugs approved and licensed are rivastigmin, donepezil, and galanthamine. Although these drugs are part of the same therapeutic class (AChEI), they differ in their pharmacology and pharmacokinetics and possess some side effects. Unfortunately, all the approved drugs for AD offer symptomatic treatment, but are unable to prevent disease progression or alter the outcome of the disease. Therefore, it is compulsory to discover new anti-Alzheimer drug candidates. To this purpose, computational approaches can be valuable in the design of new compounds with improved pharmacological profile. Molecular dynamics, molecular docking and some other in silico studies have been reported targeting AChE.[6–8] Ligand docking is designed to find the best mode of interaction between a small ligand and a large macromolecular receptor and represents one of the most widely used tools in ligand and drug design/screening. Molecular dynamics simulation, on the other hand, is a successful and well-established method in the computational study of structure and dynamics of biological macromolecules.

From the chemical point of view, xanthones represent a class of oxygenated heterocyclic compounds with a dibenzo-γ-pyrone scaffold. Its privileged structure is broadly distributed in Nature and display a wide range of biological activities, such as antibacterial, anti-inflammatory, antitumoral and α-glucosidase inhibitory activities.[9-12] Xanthones can be considered as biocompatible structures since their derivatives are capable of interacting with several different targets.[13] Currently, these class of compounds (natural and synthetic) that act on molecular targets of neurodegenerative diseases are grounds for study and exploration.[14,15] Particularly, xanthones derivatives as anti-cholinesterase agents have received significant attention in the last years (**Figure 1**).[16-19]

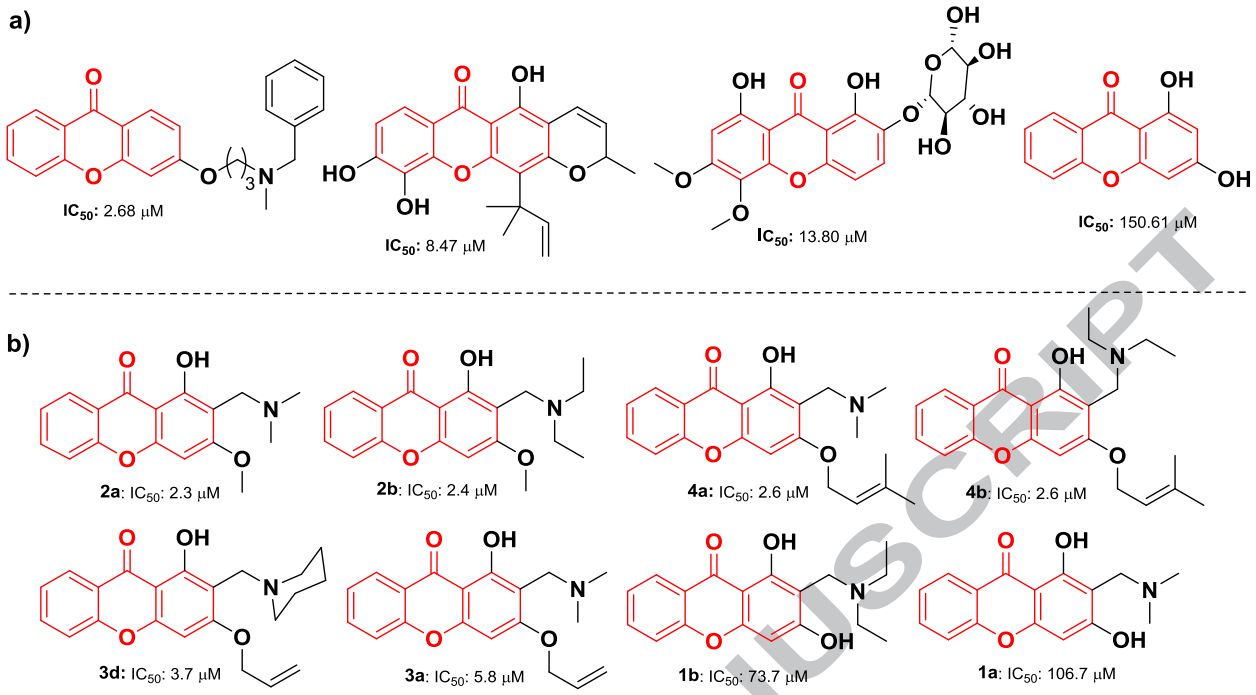

Figure 1. Figure 1. a) Some representative structures of xanthone derivatives with AChE inhibitory activity. **b**) 1,3-dihydroxyxanthone Mannich base derivatives with anti-AChE activity.

In a recent work, a series of novel 1,3-dihydroxyxanthone Mannich bases derivatives have been identified as anti-AChE agents (**Figure 1b**).[20] Within this context, we decided to carry out molecular docking simulations and molecular dynamics simulations with the aim of establishing the molecular basis for the interaction between these compounds and AChE, in order to understand and rationalize the previous experimental results. In addition, we perform rational modifications on this kind of compounds in order to improve their inhibitory effect. Finally, a new series of 1,3-dihydroxyxanthone derivatives was synthesized and their inhibitory effects on AChE were evaluated.

2. Results and Discussion

2.1 Rational design

In this section, we present the results of the computational studies we performed in order to rationalize the binding mode of the already proposed xanthonic ligands and to reengineer them

with the aim of obtaining ligands with improved affinity (we refer the reader to the Experimental section for the description of the techniques employed).

We employed docking studies to rationalize the interaction mode of a series of 1,3-dihydroxylated xanthone derivatives (**Figure 1b**). Such studies indicated that these molecules generally interacted with residues from the bottleneck region such as Phe 330, residues from peripheral anionic site (PAS) as Tyr 334 and Asp 72, while the interaction with Trp 84 from the catalytic active site (CAS) was always present (**Figure 2**).

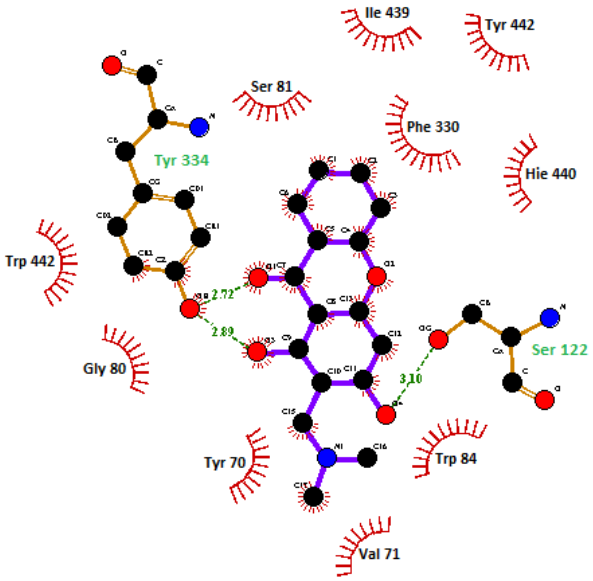

Figure 2. 2D depiction of **1a** docked into the binding site of AChE highlighting the protein residues that form the main interactions with the different structural units of the inhibitor. Hydrogen-bonding interactions are represented with green broken lines.

In order to determine the residues that most contribute to the ligand-enzyme interaction we performed free energy calculations by means of the MM/GBSA method (as implemented in the mm_pbsa program of the AMBER 12 package). This analysis enabled us to identify the π-stacking interaction of Trp 84 as the most relevant in all complexes studied. Additionally, we detected a possible salt bridge interaction involving Glu 199, which appeared intermittently in time for some of the Mannich derivatives (for example in compound **2a**). Nonetheless, this interaction was established in detriment of other ones, as for example that of Trp 432 in the case of **2a**.

In **Figure 3.a**, we display the way in which the distance between the N atom of **2a** and the O atom of the lateral chain of Glu 199 varies with time. In **Figures 3.b** and **3.c**, we show the free-energy per residue decomposition for the complex AChE-**2a**. **Figure 3.b** corresponds to the period of time that goes from 0 to 4 ns, when the interaction with Glu 199 is established (in detriment of other interactions). In turn, **Figure 3.c** corresponds to the time window that spans from 5 to 10 ns, where the energetically most significant interaction is the one formed by Trp 84.

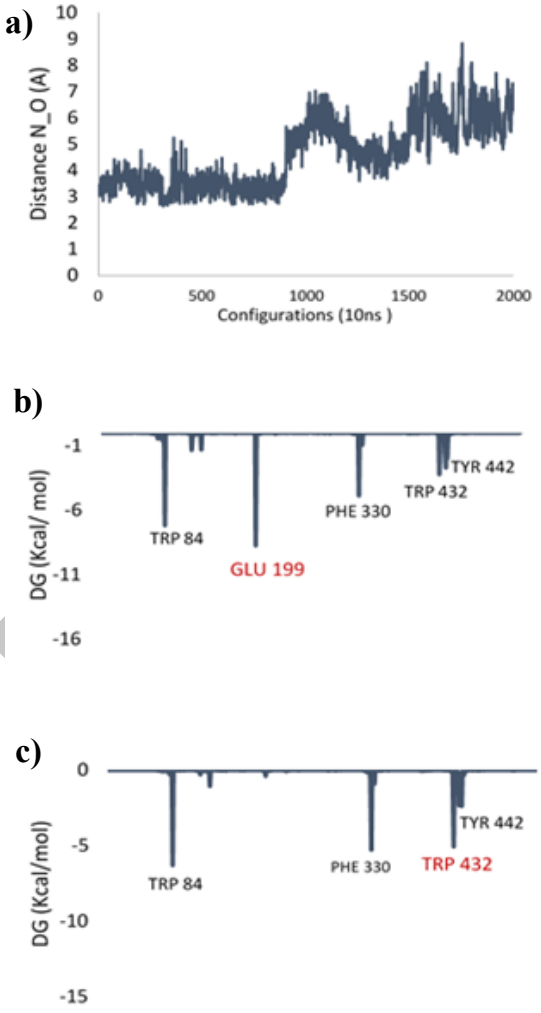

Figure 3. **a**) Distance between the N atom of **2a** and the O atom of the lateral chain of Glu 199. **b)** and **c)** Free-energy per residue decomposition for the complex AChE-**2a**. The period of time that goes from 0 to 4 ns is shown in **b)**; while period of time between 5 to 10 ns is shown in **c)**.

We also provide a correlation of the free-energy values and the activity values reported for 8 compounds of this series. The data yielded a correlation with a R^2 value of 0.65 (**Table S1**: see supplementary material).

Finally, a GIST study (Analysis of water thermodynamics using Grid Inhomogeneous Solvation) [21] allowed us to obtain the hydration map for the binding site of these compounds in AChE. This approach determined the existence of regions with high energy waters, that is, "easily removable" water. Such regions were determined as that with a water density more than 1.9 times larger than that of the bulk and with free energy values lower than DeltaG – 0.5 (Kcal/mol).[22] Then, we superimposed the configurations adopted by the different ligands in their complexes with AChE and the water map already generated. Thus, we quantified the number of water "boxes" that each ligand displaces upon binding and we employed this value as a second score function.

The protein hydration map was performed for three different time periods:

1) From 0 to 20 ns, with a spacing between consecutive configurations of 1 ps.

2) From 0 to 100 ns, with a spacing between consecutive configurations of 5 ps.

3) From 100 to 120 ns, with a spacing between consecutive configurations of 1 ps.

On the other hand, we defined two kinds of configurations for each ligand:

A) Binding mode obtained from the molecular docking simulations.

B) Starting from the docking results we performed molecular dynamics simulations and then we selected configurations for each ligand after constant root mean squared displacement (RMSD) values were reached.

We obtained good correlations for the three-time periods under study when the configurations of the different compounds were obtained by means of molecular dynamics simulations (**B**). The correlation values obtained were $R^2 = 0.78$ for the first-time span considered and $R^2 = 0.75$ for the second and third time periods. In the case of the configurations obtained directly from molecular docking simulations, the correlation values were: $R^2 = 0.7$, 0.63 and 0.58 for the three respective time periods studied (**Table S1**: see supplementary material).).

Finally, on the basis of the hydration map of the GIST study, we qualitatively evaluated the ability of the different compounds to appropriately mimic the role of the water molecules they displace upon complex formation. For example, we evaluated their ability to locate hydrophilic atoms or groups in regions where water is "strongly bonded". To this end, we generated a map for

water molecules whose energy was less than -0.5 (Kcal/mol) and we superimposed this map with the configurations obtained from the MD of each ligand. In all cases, we could realize that the hydroxyl group in position 1 is located in a region where water interacts favourably with the protein. The same happens with the oxygen atom of the carbonyl and the oxygen from the ether/hydroxyl in position 3 of the xanthonic backbone (**Figure 4**).

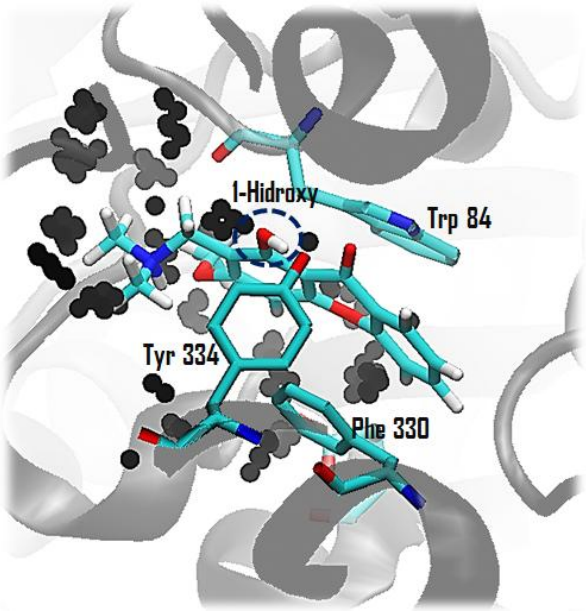

Figure 4. Complex between **2a** and AChE. Cyan: **2a** and AChE residues side chains. Dark gray spheres: regions where water is "strongly bonded".

In summary, by means of free energy calculations we were able to identify two main interaction regions. In one hand, the fused tricyclic system interacting by means of π-stacking with **Trp 84** and **Phe 330**, and by hydrogen bond with **Tyr 334**. On the other hand, the positively charged region of the amine group with the ability to interact via a salt bridge with **Glu 199**.

Additionally, the qualitative results from the GIST study (map of strongly bonded water) point to the fact of the relevance of preserving the hydroxyl (or other hydrophilic substituent) in position 1 given its capability to appropriately replace the water molecules at such region while also being able to interact with residues of the protein (**Tyr 334**).

Through Molecular Dynamics simulation studies was observed that Mannich bases studied oscillate between these two interaction regions, but they are unable to satisfy or interact with both

sites simultaneously. Thus, an appropriate reengineering of these compounds to achieve this goal is expected to improve their activity.

2.2 Proposal of new xanthone derivatives

In the light of the former results we proposed a new series of 1,3-dihydroxylated xanthone analogues, appropriately substituted in order to interact simultaneously with both regions. On the one side, this compound interacts by π-stacking via the fused tricyclic system with Trp 84 and Phe 330, while establishing a hydrogen bond with Tyr 334 by means of the hydroxy group in position 1. On the other hand, given the introduction of an appropriate linker, its positively charged amino group is now able to form a salt bridge with Glu 199. A series of additional interactions, mainly of hydrophobic nature should be included (interactions already present in the Mannich bases). Thus, theoretical studies for a series of derivatives with the proposed motif presented in **Figure 6** were performed.

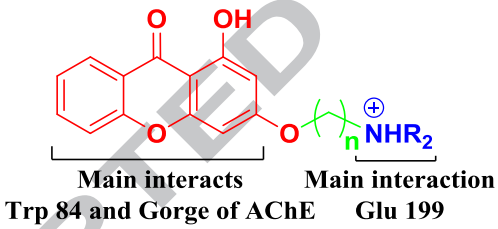

Compound	Linker	Amino group
6	3	diethylamine
7	4	diethylamine
8	5	diethylamine
9	6	diethylamine
10	5	pyrrolidine
11	5	piperidine
12	5	morpholine

Figure 5. Proposed motif for new 1,3-dihydroxyxanthone derivatives.

The linker lengths studied varied between 3 and 6 methylenes, including ethyl groups as substituents in the charged group. In **Figure 5**, we include all new compounds theoretically (by means of Molecular Docking and Molecular Dynamics) and/or empirically evaluated. In supplementary material, we include Molecular Docking results (Score functions) for an expanded series of compounds, including some different amine groups for each linker length.

Table 2. Amphiphilic xanthones **6-12** biologically tested.

Compound	Linker lenght	Amino group	$IC_{50} \pm SD$ (μM)

6	3	diethylamine	3.29 ± 0.26
7	4	diethylamine	4.86 ± 0.50
8	5	diethylamine	0.69 ± 0.10
9	6	diethylamine	2.37 ± 0.33
10	5	pyrrolidine	0.95 ± 0.19
11	**5**	**piperidine**	**0.46 ± 0.02**
12	5	morpholine	12.09 ± 1.87
***tacrine*[a]**	-	-	0.029 ± 0.003

[a] Reference inhibitor.

The results of the molecular docking revealed the ability of all the compounds to interact electrostatically (salt bridge) with Glu 199, while the interactions of the fused tricyclic system were similar to that of the former Mannich analogues. That is, this series of new analogues preserve the interactions present in the 1,3-dihydroxylated xanthonic Mannich derivatives but also add the electrostatic interaction. On the other hand, and given the structural similarity of the xanthonic skeleton with tacrine (reference inhibitor), we compared their modes of interaction with AChE. The position and interactions of the fused tricyclic system of different xanthones studied were similar to tacrine (**Figure 6a**), although it is important to mention that tacrine is able to form a hydrogen bond interaction with the His 440 (**Figure 6b**), while xanthones do not exhibit this interaction.

In order to estimate the activity range for the new xanthone derivatives and to determine the optimal linker length, we performed free energy calculations (GBSA) and, in the same way as done for the xanthonic Mannich derivatives, we calculated the quantity of low energy water "boxes" displaced by each of the new proposed analogues (**Table1**). The latter study was conducted again over three different time periods and for ligand configurations obtained both directly for the molecular docking results (**A**) and for the respective molecular dynamics simulations (**B**). From the results of **Table 1**, we concluded that the better lengths for the linker would be 5 or 6 methylenes.

Table 1. Results of new 1,3-dihydroxyxanthone derivatives theoretically evaluated.

Compound	Score docking	GBSA (Kcal/mol)	BOX-1A*	BOX-1B*	BOX-2A*	BOX-2B*	BOX-3A*	BOX-3B*
6	-11.41	-28.67	279	169	294	178	305	183
7	-11.92	-36.6	418	280	435	293	431	296
9	-12.55	-49.18	429	418	442	413	443	415
8	-12.3	-48.7	416	334	430	350	426	381

(*) Number of water "easily removable boxes". 1A, 1B, 2A, 2B, 3A and 3B refers to time periods and kinds of configurations (Docking or Molecular Dynamics).

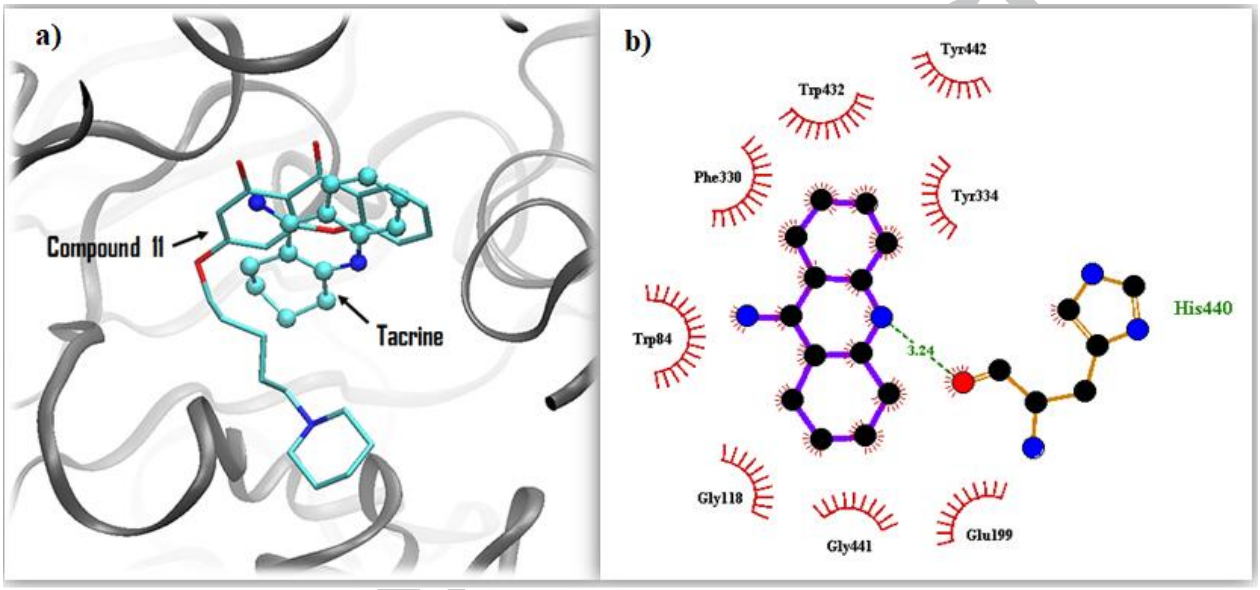

Figure 6. A) Superposition of compound 11 (bonds) and tacrine (CPK) both in complex with AChE. **B**) 2D depiction of tacrine in complex with AChE (PDB: 1ACJ) highlighting the protein residues that form the main interactions with the different structural units of the inhibitor. Hydrogen-bonding interactions are represented with green broken lines.

Also, we carried out a decomposition of the free energy change per residue in order to quantify the possible interactions for each ligand–AChE complex. **Figure 7**displays, superimposed, the free energy decompositions for the different complexes. From the free energy values of the interaction with Glu 199, we could infer that the optimal linker length would be that of five methylenes.

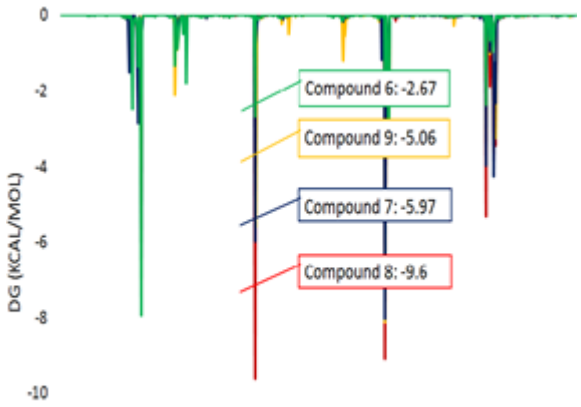

Figure 7. Free energy values for the interaction between compounds **6-9** with Glu 199.

In order to contrast with the theoretical results, we performed the synthesis of this new series of compounds **6-9** and their activities as AChE inhibitors were experimentally determined by Ellman's method (**Table 2**).[23] Finally, taking into account that compound **8**, with a five methylenes linker, gave the best experimental results (lowest IC_{50}), and based on the results of molecular docking (see supplementary material), we expanded the series by changing the charged amino group to obtain compounds **10-12**.

2.3 Chemistry

The synthesis of hydroxylated xanthone **1** was achieved according to the general reaction pathway outlined in **Scheme 1**. The building block **1** was obtained by one-pot synthesis using Eaton's reaction. In Eaton's protocol, **1** was obtained by the condensation of 2-hydroxybenzoic acid with phloroglucinol in the presence of a mixture of phosphorus pentoxide-methanesulfonic acid (Eaton's reagent) as condensing agent (**Scheme 1**).[24] The precursor xanthone **1** was obtained as a yellow solid (yield 70%) after purified by column chromatography using silica gel 60.

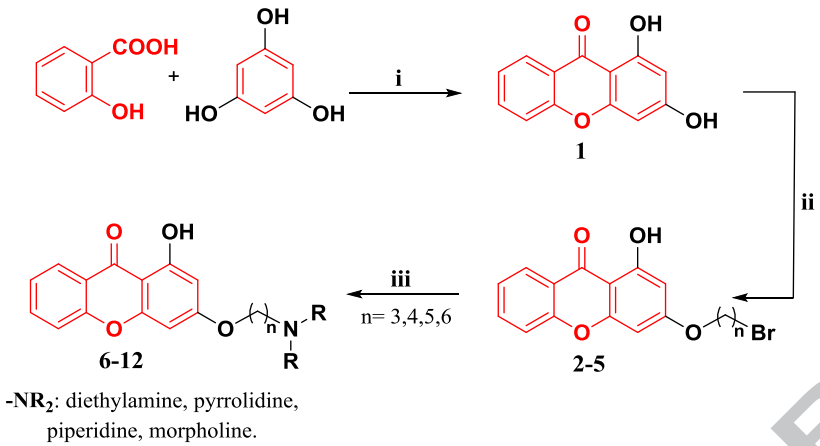

Scheme 1. Synthesis of 1-hydroxyl-3-aminoalkoxy xanthone derivatives **6-12**. *Reagents and conditions*: (**i**) P_2O_5, methanesulfonic acid, 80 °C, 2 h; (**ii**) $Br(CH_2)_nBr$, K_2CO_3, dry acetone, r.t, 24 h; (**iii**) secondary amine, dry acetone, r.t, 24 h.

The subsequent etherification of the hydroxyl group in the position 3 of 1,3-dihydroxyxanthone (**1**) with dibromoalkanes was carried out in K_2CO_3/dry acetone to offer the key intermediates **2-5**, which possessed various side chains with different length. Then, compounds **2-5** were treated with appropriate secondary amines at room temperature in the presence of dry acetone to give the target compounds **6- 12** in very good yield (75-92%).[25] The new compound **6**, **8**, **9**, **11** and **12** were fully characterized by IR and NMR. The NMR assignments are provided explicitly in the Experimental section.

2.4 Biology

From **Table 2**, we could see that the theoretical predictions on the chain length were correct since the best activity within the test series was achieved by compounds **8**, **10** and **11**. Among them, compound **11**, with a piperidine moiety as the amino group, elicited the strongest AChE inhibition. These results indicate that the 1,3-dihydroxyxanthone derivatives proposed in this work do in fact improve the experimental affinity as compared to the previously proposed Mannich bases. Compound **12** turned out to be the weakest inhibitor of the series, even though the linker

was five methylenes long. This result can be explained by the presence of a second heteroatom in the amino group. The electron-withdrawing effect of the oxygen atom might reduce the electronic density of the tertiary amine, thereby affecting protonation, which could, in turn, diminish the interaction between the ammonium and Glu199. A similar effect was observed by Li *et al*. for flavonoids linked to cyclic amines possessing an additional nitrogen or oxygen atom in the terminal group.[26] Also, we have observed the same effect in morpholine derivatives of cativic acid, a diterpenoid with moderate AChE inhibition.[27]

Table 2. Amphiphilic xanthones **6-12** biologically tested.

Compound	Linker lenght	Amino group	$IC_{50} \pm$ SD (μM)
6	3	diethylamine	3.29 ± 0.26
7	4	diethylamine	4.86 ± 0.50
8	5	diethylamine	0.69 ± 0.10
9	6	diethylamine	2.37 ± 0.33
10	5	pyrrolidine	0.95 ± 0.19
11	**5**	**piperidine**	**0.46 ± 0.02**
12	5	morpholine	12.09 ± 1.87
tacrine[a]	-	-	0.029 ± 0.003

[a] Reference inhibitor.

In turn, the expected activity range is consistent for the analogues with linkers with 5 and 6 methylene length. The remaining analogues (linkers with 3 or 4 methylenes) while yielding affinities lower than the ones with 5 or 6 methylenes, presented better experimental inhibition values in comparison with the theoretical expectations.

2.5 Perspectives for future work

For the configuration adopted in the theoretical studies by the analogue with the overall best activity, compound **11**, we superimposed the strongly bonded water map or low-energy water (the theoretical configuration was that adopted in the molecular dynamics once the RMSD values get constant). In this way, we verified (**Figure 8**) that in general the positions with tightly bound water are well compensated by the ligand except that in the linker region. Thus, we could modify

the chemical nature of the linker (make it more hydrophilic) and thus possibly increase the inhibitory potency of this analogue.

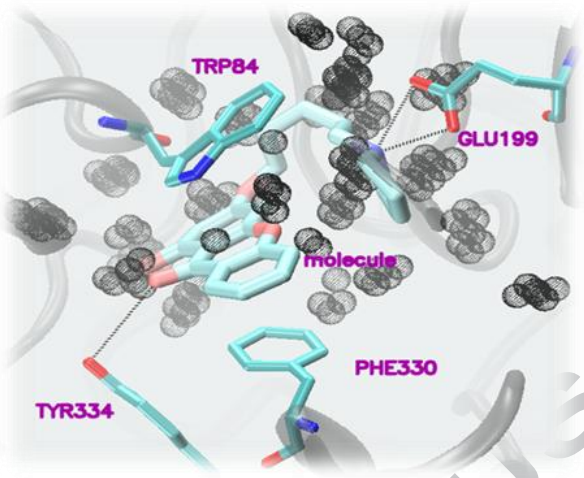

Figure 8. Complex between **11** and AChE. Cyan: **11** and AChE residues side chains. Dark gray spheres: regions where water is "strongly bonded".

3. Conclusions

In summary, the theoretical studies presented in this work nicely rationalize the binding mode to AChE of already proposed Mannich bases[20] and enabled us to successfully reengineer them towards lead compounds of mildly improved affinity (roughly one order of magnitude enhancement), as accurately confirmed by the biological assays we also hereby provide. In this context, a new series of 1,3-dihydroxyxanthone derivatives were easily synthesized by modifications to known procedures[25] and subsequently biologically evaluated against AChE. In particular, amphiphilic xanthone **11** showed the best inhibitory effect (IC_{50}: 0.46 μM), which could be considered as a useful prototype for further development of new anti-AD agents..

4. Experimental

4.1. *General*

All operations were performed under an argon atmosphere using standard Schlenk techniques. Solvents were dried and distilled in accordance with standard procedure.[28] Reactions were monitored by thin-layer chromatography (TLC) on silica gel plates (60F-254) visualized under UV light and/or using 5% phosphomolybdic acid in ethanol. All ^{1}H and ^{13}C NMR spectra were

recorded at room temperature in $CDCl_3$, DMSO-d_6 or Acetone-d_6 on a Bruker Avance ARX-300 spectrophotometer. Chemical shifts (δ) are reported in parts per million (ppm) from tetramethylsilane (TMS) using the residual solvent resonance ($CDCl_3$: 7.26 ppm for ^{1}H NMR and 77.16 ppm for ^{13}C NMR; DMSO-d_6: 2.50 ppm for ^{1}H NMR and 39.50 ppm for ^{13}C NMR; Acetone-d_6: 2.09 ppm for ^{1}H NMR, 30.60 and 205.87 ppm for ^{13}C NMR). Multiplicities are abbreviated as follows: s = singlet, d = doublet, t = triplet, q = quartet, m = multiplet; brs = broad signal). IR spectra were recorded on a Perkin-Elmer Paragon 1000 FT-IR spectrometer in the ATR mode at room temp. Melting points were determined using a Büchi 510 apparatus and are not corrected. UV spectra were recorded on a JASCO V-630BIO spectrophotometer. Mass spectra (EI) were obtained at 70 eV on an Agilent CG-78903 instrument equipped with a MS-5977A MSD selective mass detector. The purity of volatile compounds and the chromatographic analyses (GC) were determined with a GC Shimadzu (GC-14B) with a flame ionization detector equipped with a HP-5MS column (30 m × 0.25 mm × 0.25 μm) using nitrogen as carrier gas. High resolution mass spectra were recorded on Thermo Fisher LTQ Orbitrap XL, (for EI) and a Finnigen MAT 95 (for ESI). Flash column chromatography was performed using Macherey Nagel MN Kieselgel 60M (0.040- 0.063 mm / 230-240 mesh ASTM). Acetylcholinesterase from electric eel (type VI-S), 5,5'-dithiobis(2-nitrobenzoic acid) (DTNB), acetylthiocholine iodide (ATCI) and tacrine were purchased from Sigma.

4.2. Synthesis of 1,3-dihydroxyxanthone (**1**)[24]

Under argon atmosphere, a mixture of phosphorus pentoxide (0.90 g, 6.35 mmol) and methanesulfonic acid (10.13 g, 15 mL, 0.10 mol) was heated on a steam bath (90 °C) until a clear solution was obtained (30 minutes). Then, a mixture of phloroglucinol (0.38 g, 3 mmol) and 2-hydroxybenzoic acid (0.46 g, 3 mmol) was added to the reaction mixture. This mixture was stirred at reflux (80 ˚C) for 1 h and the progress of the reaction was monitored by TLC. After completion, the reaction mixture was poured into ice-water. The resulting orange solid was collected by filtration, washed with water, dried in air, and the residue was then purified by

column chromatography using silica gel 60. The desired product **1** (0.48 g, 2.1 mmol, 70%) was eluted with hexane/EtOAc (90:10) as a yellow solid. m.p.: 255-257 °C; ^{1}H NMR (300 MHz, DMSO-d_6): δ 6.20 (d, J = 2.1 Hz, 1 H), 6.37 (d, J =2.1 Hz, 1 H), 7.42-7.45 (m, 2 H), 7.55 (td, J = 8.0 Hz, 1 H), 8.10 (dd, J = 8.0, 1 H, 1.5 Hz), 11.07 (s, 1 H), 12.80 (s, 1 H). ^{13}C NMR (DMSO-d_6, 75 MHz): δ 95.1, 99.1, 103.1, 118.2, 120.7, 125.3, 126.6, 135.7, 156.4, 158.1, 163.8, 165.2, 180.4. IR (KBr): ν 3327, 1654, 1610, 1570, 1491, 1470, 1445, 1222, 1163, 1078, 827, 762 cm^{-1}.

4.2.1 General procedure for the synthesis of 3-bromoalkoxy substituted xanthones (**2-5**)

Under argon atmosphere, a mixture of **1** (100 mg, 0.4 mmol) and K_2CO_3 (110 mg, 0.8 mmol) in dry acetone (2 mL), 1,*n*-dibromoalkane (0.6 mmol, n > 2) was slowly added by syringe. The reaction mixture was stirred at room temperature for about 24 h, with monitoring by TLC. The reaction mixture was poured into ice-water. The resulting yellow solid was collected by filtration, washed with water, dried in air, and the residue was then purified by column chromatography using silica gel 60. The compounds **2-5** were eluted with hexane/EtOAc (95:5) as yellow solids.

***3-(3-Bromopropoxy)-1-hydroxy-9H-xanthen-9-one* (2)**[25]

Isolated yield: 60% (pale yellow solid) from compound **1** and 1,3-dibromopropane. m.p.: 119-121 °C; ^{1}H NMR (300 MHz, $CDCl_3$): δ 2.28-2.39 (m, 2H), 3.54 (t, 2H), 4.12 (t, 2H), 6.34 (d, 1H), 6.43 (d, 1H), 7.42-7.44 (m, 2H), 7.71 (ddd, 1H), 8.24 (dd, 1H), 12.85 (s, 1H, OH). ^{13}C NMR (75 MHz, $CDCl_3$): δ 29.6, 30.0, 66.0, 93.2, 97.5, 104.1, 117.6, 120.1, 124.1, 125.9, 135.1, 156.1, 157.7, 163.6, 165.8, 180.8. IR (KBr): ν 3450, 2965, 1660, 1611, 1575, 1465, 1297, 1160, 1037, 828 cm^{-1}.

***3-(4-Bromobutoxy)-1-hydroxy-9H-xanthen-9-one* (3)**[25]

Isolated yield: 45% (yellow solid) from compound **1** and 1,4-dibromobutane. m.p.: 132-135 °C; ^{1}H NMR (300 MHz, $CDCl_3$): δ 2.76-2.79 (m, 4H), 3.63 (t, 2H), 4.25 (t, 2H), 6.38 (d, 1H), 6.59 (d, 1H), 7.49 (m, 1H), 7.56 (d, 1H), 7.87 (ddd, 1H), 8.23 (dd, 1H), 12.88 (s, 1H, OH). ^{13}C NMR (75 MHz, $CDCl_3$): δ 27.7, 29.4, 33.3, 67.6, 93.2, 97.5, 104.0, 117.6, 120.6, 124.1, 125.9, 135.5,

156.1, 157.8, 163.6, 166.1, 180.8. IR (KBr):ν 3546, 2959, 1663, 1609, 1572, 1469, 1299, 1158, 1081, 824 cm^{-1}.

***3-(5-Bromopentyloxy)-1-hydroxy-9H-xanthen-9-one* (4)**[25]

Isolated yield: 50% (yellow solid) from compound **1** and 1,5-dibromopentane. m.p.: 130-132 °C; ^{1}H NMR (300 MHz, $CDCl_3$): δ 1.31-1.40 (m, 2H), 1.85-2.00 (m,4H), 3.46 (t, 2H), 4.01 (t, 2H), 6.33 (d,1H), 6.41 (d, 1H), 7.34-7.40 (m, 2H), 7.70 (ddd, 1H), 8.24 (dd, 1H), 12.85 (s, 1H, OH). ^{13}C NMR (75 MHz, $CDCl_3$): δ 24.8, 28.3, 32.5, 33.5, 68.3, 93.3, 97.5, 104.1, 117.7, 124.1, 126.1, 128.0, 135.1, 156.1, 157.8, 163.7, 166.3, 180.9. IR (KBr): ν 3460, 2946, 1661, 1609, 1573, 1481, 1296, 1163, 1038, 820 cm^{-1}.

***3-(6-Bromohexyloxy)-1-hydroxy-9H-xanthen-9-one* (5)**[25]

Isolated yield: 45% (yellow solid) from compound **1** and 1,6-dibromohexane. m.p.: 139-141 °C; ^{1}H NMR (300 MHz, $CDCl_3$): δ 1.35-1.58 (m, 4H), 1.81-1.92 (m, 4H), 3.40 (t, 2H), 4.03 (t, 2H), 6.31 (d, 1H), 6.39 (d, 1H), 7.36-7.41 (m, 2H), 7.66 (ddd, 1H), 8.24 (dd, 1H), 12.85 (s, 1H, OH). ^{13}C NMR (75 MHz, $CDCl_3$): δ 25.3, 27.9, 28.9, 32.7, 33.8, 68.5, 93.3, 97.5, 103.9, 117.7, 120.7, 124.1, 125.9, 135.0, 157.8, 163.7, 165.1, 166.3, 180.8. IR (KBr): ν 3430, 2945, 1662, 1602, 1573, 1462, 1296, 1179, 1074, 823 cm^{-1}.

4.2.2. General procedure for the synthesis of 1-hydroxy -3-aminoalkoxy xanthone derivatives (**6-12**)

Under argon atmosphere, a mixture of **2-5** (1 mmol) in dry acetone (1 mL), corresponding secondary amine (diethylamine, pyrrolidine, piperidine or morpholine, 2.5 mmol) was added dropwise by a syringe. The resulting solution was stirred at room temperature until the completion of the reaction (24-48 h). The progress of the reaction was monitored by TLC. The reaction mixture was poured into ice-water. The resulting yellow solid was collected by filtration, washed with water, and then dried in vacuo to give compound **6-12** respectively without further purification.

3-(3-(diethylamino)propoxy)-1-hydroxy-9H-xanthen-9-one (**6**)

Isolated yield: 85% (yellow solid) from compound **2** and diethylamine. m.p.: 190-191 °C; ^{1}H NMR (300 MHz, $CDCl_3$): δ 1.06 (t, 6H), 1.82- 1.86 (m, 2H), 2.42- 2.48 (m, 4H), 2.55- 2.59 (m, 2H), 4.05 (t, 2H), 6.34 (d, 1H), 6.41 (d, 1H), 7.45- 7.50 (m, 2H), 7.71 (ddd, 1H), 8.23 (dd, 1H), 12.85 (s, 1H, OH). ^{13}C NMR (75 MHz, $CDCl_3$): δ 8.8, 29.6, 47.1, 49.2, 65.5, 93.1, 97.5, 104.2, 117.5, 120.3, 124.2, 125.9, 135.1, 156.1, 157.8, 163.5, 165.2, 180.9. IR (film): ν 3430, 3055, 2986, 1653, 1606, 1468, 1265, 1169, 824, 743 cm^{-1}. HRMS (EI) m/z: 341.1627 calcd for $C_{20}H_{23}NO_4$, found 341.1631.

3-(4-(Diethylamino)butoxy)-1-hydroxy-9H-xanthen-9-one (**7**)[25]

Isolated yield: 80% (yellow solid) from compound **3** and diethylamine; m.p: 181-183°C; ^{1}H NMR (300 MHz, $CDCl_3$): δ 1.14 (t, 6H), 1.70-1.75 (m, 2H), 1.77- 1.84 (m, 2H), 2.91-3.02 (m, 6H), 4.18 (t, 2H), 6.43 (d, 1H), 6.67 (d, 1H), 7.60- 7.65 (m, 1H), 7.73 (d, 1H), 7.90 (ddd, 1H), 8.17 (dd, 1H), 12.81 (s, 1H, OH). ^{13}C NMR (75 MHz, $CDCl_3$): δ 8.7, 20.6, 26.2, 46.8, 51.2, 67.5, 93.0, 97.3, 103.9, 117.5, 120.5, 124.0, 125.7, 135.1, 155.9, 157.7, 165.6, 163.4, 180.7. IR (film): ν 3432, 3051, 2985, 1650, 1603, 1465, 1262, 1170, 823, 745 cm^{-1}. HRMS (EI) m/z: 355.1784 calcd for $C_{21}H_{25}NO_4$, found 355.1789.

3-((5-(diethylamino)pentyl)oxy)-1-hydroxy-9H-xanthen-9-one (**8**)

Isolated yield: 80% (yellow solid) from compound **4** and diethylamine. m.p.: 150-151°C, ^{1}H NMR (300 MHz, $CDCl_3$): δ 1.05 (t, 6H), 1.51-1.70 (m, 4H), 1.82-1.93 (m, 2H), 2.48-2.52 (m, 6H), 4.05 (t, 2H), 6.34 (d, 1H), 6.41 (d, 1H), 7.45- 7.51 (m, 2H), 7.71 (ddd, 1H), 8.23 (dd, 1H), 12.85 (s, 1H, OH), ^{13}C NMR (75 MHz, $CDCl_3$): δ 24.1, 26.8, 29.1, 47.1, 52.9, 68.7, 93.3, 97.6, 104.2, 117.8, 124.1, 126.1, 135.0, 156.4, 157.8, 163.3, 166.5, 180.9, IR (film): ν 3440, 2964, 2790, 1660, 1603, 1571, 1472, 1329, 1298, 1179, 1079, 821, 758 cm-1. HRMS (EI) m/z: 369.1940 calcd for $C_{22}H_{27}NO_4$, found 369.1944.

3-((6-(diethylamino)hexyl)oxy)-1-hydroxy-9H-xanthen-9-one (**9**)

Isolated yield: 75% (yellow solid) from compound **5** and diethylamine. m.p.: 110-111 °C; ^{1}H NMR (300 MHz, $CDCl_3$): δ 1.06 (t, *J* = 8.0 Hz, 6H), 1.24 –1.34 (m, 2H), 1.42–1.55 (m, 4H), 1.80 (tt, *J* = 7.9, 4.7 Hz, 2H), 2.42 (t, *J* = 7.6 Hz, 2H), 3.01 (q, *J* = 8.0 Hz, 4H), 4.11 (t, *J* = 4.7 Hz, 2H), 6.37 (d, *J* = 1.9 Hz, 1H), 6.60 (d, *J* = 2.1 Hz, 1H), 7.26 – 7.35 (m, 2H), 7.56 (td, *J* = 7.5, 2.0 Hz, 1H), 8.00 (dd, *J* = 7.5, 2.0 Hz, 1H), 12.71 (s, 1H, OH). ^{13}C NMR (75 MHz, $CDCl_3$): δ 8.7, 23.4, 25.6, 26.7, 28.8, 29.8, 46.5, 51.3, 68.5, 93.2, 97.5, 103.9, 117.6, 120.7, 124.1, 125.9, 135.1, 156.1, 157.8, 163.6, 166.3, 180.9. IR (film): ν 3445, 2955, 1665, 1605, 1571, 1468, 1320, 1170, 824, 747 cm^{-1}. HRMS (EI) m/z: 383.2097 calcd for $C_{23}H_{29}NO_4$, found 383.2093.

1-Hydroxy-3-(5-(pyrrolidin-1-yl)pentyloxy)-9H-xanthen-9-one (**10**)[25]

Isolated yield: 92% (pale yellow solid) from compound **4** and pyrrolidine. m.p.: 105- 106°C; ^{1}H NMR (300 MHz, $CDCl_3$): δ 1.47-1.54 (m, 2H), 1.56-1.63 (m, 2H), 1.74-1.80 (m, 4H), 1.81-1.87 (m, 2H), 2.44-2.52 (m, 6H), 4.03 (t, 2H), 6.31 (d, 1H), 6.39 (d, 1H), 7.33- 7.38 (m, 1H), 7.40 (d, 1H), 7.69 (ddd, 1H), 8.22 (dd, 1H), 12.82 (s, 1H, OH). ^{13}C NMR (75 MHz, $CDCl_3$): δ 23.5, 24.3, 28.8, 29.0, 54.3, 56.5, 68.7, 93.3, 97.6, 103.9, 117.7, 120.4, 124.1, 126.0, 135.0, 156.2, 157.8, 163.7, 166.4, 180.9. IR (film): ν 3430, 2949, 2793, 1662, 1608, 1571,1468,1316,1299,1166, 1082, 824, 763 cm^{-1}. HRMS (EI) m/z: 367.1784 calcd for $C_{22}H_{25}NO_4$, found 367.1789.

1-hydroxy-3-((5-(piperidin-1-yl)pentyl)oxy)-9H-xanthen-9-one (**11**)

Isolated yield: 80% (yellow solid) from compound 4 and piperidine. m.p.: 101- 102 °C; ^{1}H NMR (300 MHz, $CDCl_3$): δ 1.26- 1.32 (m, 2H), 1.40-1.68 (m, 8H), 1.76-1.82 (m, 2H), 2.30-2.35 (m, 6H), 4.05 (t, 2H), 6.34 (d, 1H), 6.42 (d, 1H), 7.32-7.37 (m, 1H), 7.44 (d, 1H), 7.71 (ddd, 1H), 8.26 (dd, 1H), 12.82 (s, 1H, OH). ^{13}C NMR (75 MHz, $CDCl_3$): δ 24.2, 24.6, 26.1, 26.8, 29.0, 54.8, 59.5, 68.7, 93.4, 97.6, 103.9, 117.8, 120.8, 124.1, 126.1, 134.9, 156.1, 157.9, 163.6, 166.4, 180.9. IR (film): ν 3430, 2930, 2853, 1661, 1607, 1568, 1468, 1298, 1175, 1078, 823, 745 cm $^{-1}$. HRMS (EI) m/z: 381.1940 calcd for $C_{23}H_{27}NO_4$, found 381.1945.

1-hydroxy-3-((5-morpholinopentyl)oxy)-9H-xanthen-9-one (**12**)

Isolated yield: 82% (yellow solid) from compound **4** and morpholine. m.p.: 130-131 °C; ^{1}H NMR (300 MHz, $CDCl_3$): δ 1.35-1.50 (m, 4H), 1.62-1.75 (m, 2H), 2.41-2.55 (m, 6H), 4.04-4.11 (m, 6H), 6.34 (d, 1H), 6.43 (d, 1H), 7.36-7.40 (m, 1H), 7.43 (d, 1H), 7.71 (ddd, 1H), 8.26 (dd, 1H), 12.82 (s, 1H, OH). ^{13}C NMR (75 MHz, $CDCl_3$): δ 24.0, 26.3, 28.9, 46.5, 59.3, 68.2, 68.6, 93.7, 97.4, 103.7, 117.6, 120.7, 124.1, 126.1, 135.1, 156.1, 157.9, 163.6, 166.3, 180.9. IR (film): ν 3432, 2941, 1654, 1609, 1568, 1466, 1319, 1266, 1168, 825, 744 cm^{-1}. HRMS (EI) m/z: 383.1733 calcd for $C_{22}H_{25}NO_5$, found 383.1738.

4.3. Biological activity

4.3.1. Cholinesterase inhibition assay

Electric eel AChE was used as source of cholinesterase. AChE inhibitory activity was measured *in vitro* by the spectrophotometric method developed by Ellman with slight modifications.[23] The lyophilized enzyme (500 U) was dissolved in buffer phosphate A (8 mM K_2HPO_4, 2.3 mM NaH_2PO_4) to obtain 5 U/mL stock solution. Further enzyme dilution was carried out with buffer phosphate B (8 mM K_2HPO_4, 2.3 mM NaH_2PO_4, 0.15 M NaCl, 0.05% Tween 20, pH 7.6) to produce 0.126 U/mL enzyme solution. Samples were dissolved in buffer phosphate B with 2.5% of MeOH as cosolvent. Enzyme solution (300 µL) and sample solution (300 µL) were mixed in a test tube and incubated for 60 min at room temperature. The reaction was started by adding 600 µL of the substrate solution (0.5 mM DTNB, 0.6 mM ATCI, 0.1 M Na_2HPO_4, pH 7.5). The absorbance was read at 405 nm for 120 s at 27 °C. Enzyme activity was calculated by comparing reaction rates for the samples to the blank. All reactions were performed in triplicate. IC_{50} values were determined with GraphPad Prism 5. Tacrine (99%) was used as the reference AChE inhibitor.

4.4. Molecular modeling

The three-dimensional structures of the different molecules under evaluation were generated by means of the program UCSF- Chimera.[29]

Molecular docking simulations of AChE from Torpedo californica (PDB: 1UT6) were performed with the Autodock 4 simulation package. The receptor structure was prepared by removing the organic molecule from the binding site together with crystallization water. The resulting structure was minimized, then Gasteiger charges were added and, finally, nonpolar hydrogen atoms were removed with the AutodockTools (ADT) program.[30] The simulation box was defined so as to include all the residues of the catalytic site, bottlenecks and the peripheral anionic site of the enzyme. This procedure generated a grill of 86 points in each of the axis (X, Y, Z) with a separation of 0.375 Å between consecutive points.

The analysis of interactions of the different complexes, as well as the 2D image, were made with LigPlot+ program.[31,32]

For the molecular dynamics (MD) simulations we employed the AMBER 12 simulation package [33] with the ff99SB force field. In all cases the complexes were placed within cubic boxes with periodic boundary conditions. The different systems were then solvated with explicit water by using the TIP3P model. Production runs for all studied complexes were performed under the NPT ensemble at a temperature of 300 K. The length of such trajectories was 10 ns, recording a total amount of 2000 configurations in each case. In turn, in order to perform the MD simulations, we had to produce the topologies for the different organic. Thus, the parametrization of the different ligands was carried out with antechamber. [34,35] Finally, the post MD analysis was made with the CPPTRAJ program.[36]

On the other hand, a solvation thermodynamic mapping study of the molecular Surface of AchE was conducted with GIST, recently included in AmberTools. We used the structure of AChE from Protein Data Bank (PDB: 1UT6). We removed the ligand from the binding site and used Tleap and other Amber Tools to assign protein parameters from the AMBER99SB force field and solvate the protein with TIP3P water molecules. The simulations used a periodic box (with at least 10 Å between any protein atom and the edge of the periodic box). Three disulfide bonds

were set up to join cysteine pairs 67/94, 254/265, 402/521. Energy minimization, followed by MD simulation, was carried out with the Amber 12 software. First, the energy of the system was minimized in two rounds (both used 1500 steps of the steepest descents algorithm followed by the conjugate gradient method for a maximum of 2000 steps). In the first round, all protein atoms were harmonically restrained to their initial positions with a force constant of 100 kcal/mol/Å2. In the second round, the system was further relaxed keeping only non-hydrogen protein atoms restrained, with the same force constant. The energy-minimized system was then heated with a series of 20 ps constant-volume and constant-temperature MD simulations with the first simulation at 50 K and the temperature incremented by 50 K every 20 ps until 300 K was reached. The system was then equilibrated for 10 ns at 300 K at a constant pressure of 1 atm. At the final volume, the system was then equilibrated for an additional 5 ns at constant volume. The final MD production run of 120 ns was performed at constant number of particles, volume, and temperature (NVT), and system configurations were stored every 1 ps, for a total of 120 000 stored configurations. Throughout each of the MD simulations, all protein atoms were harmonically restrained to their positions following the energy minimization step, with a force constant of 100 kcal/mol/Å. The SHAKE algorithm was used to constrain the lengths of all bonds involving hydrogen atoms. Temperature was regulated by Langevin dynamics with a collision frequency of 2.0 ps^{-1}. A 9 Å cutoff was applied to all nonbonded interactions. Then, the main GIST solvation maps were produced from these configurations.

Declaration of interest

The authors report no conflicts of interest.

Acknowledgments

This work was generously supported by the Consejo Nacional de Investigaciones Científicas y Técnicas (CONICET), Agencia Nacional de Promoción Científica y Tecnológica (ANPCyT) and

Universidad Nacional del Sur (UNS) from Argentina. SA, APM, DCG and GAA are research members of CONICET. CAM and BB thank the CONICET for a doctoral fellowship.

Appendix A. Supplementary data

Supplementary data associated with this article can be found at http://

References

1. Walsh, D. M.; Selkoe, D. J. *Neuron*, **2004**, *44*, 181-193.

2. Léon, R.; Garcia, A. G.; Marco-Contelles, J. *Med. Res. Rev*. **2013**, *33*, 139-189.

3. Agis-Torres, A.; Söllhuber, M.; Fernandez, M.; Sanchez-Montero, J. M. *Curr. Neuropharmacol*. **2014**, *12*, 2-26.

4. Ling, R.; Yoshida, M.; Mariano, P. S. *J. Org. Chem.* **1996**, *61*, 4439–4449.

5. Singh, M.; Kaur, M.; Kukreja, H.; Chugh, R.; Silakari, O.; Singh, D. *Eur. J. Med. Chem*. **2013**, *70*, 165-188.

6. a) Goering, B. K. Ph.D. Dissertation, Cornell University, **1995**. b) Selkoe, D. J. *Science* **2012**, *337*, 1488-1492.

7. Tai, K.; Shen, T.; Henchman, R. H.; Bourne, Y.; Marchot, P.; McCammon, J. A. *J. Am. Chem. Soc.* **2002**, *124* (21), 6153-6161.

8. Kua, J.; Zhang, Y.; McCammon, J. A. *J. Am. Chem. Soc.* **2002**, *124* (28), 8260-8267.

9. Pilger, C.; Bartolucci, C.; Lamba, D.; Tropsha, A.; Fels, G. *J. Mol. Graph. Model*. **2001**, *19*, 288-296.

10. Na,Y. *J. Pharm. Pharmacol.* **2009**, *61*, 707–712.

11. Gao, X. M.; Yu, T.; Cui, M. Z.; Pu, J. X.; Du, X.; Han, Q. B.; Hu, Q. F.; Liu, T. C.; Luo, K. Q.; Xu, H. X. *Bioorg. Med. Chem. Lett* **2012**, 22, 2350-2353.

12. Pinto, M. M.; Sousa, M. E. *Curr. Med. Chem*. **2005**, *12*, 2517–2538.

13. Li, G. L.; He, J. Y.; Zhang, A. Q.; Wan, Y. Q.; Wang, B. Chen, W. H. *Eur. J. Med. Chem*. **2011**, *46*, 4050–4055.

14. Negi, J. S.; Bisht, V. K.; Singh, P.; Rawat, M. S. M.; Joshi, G. P. *J. Appl. Chem*. **2013**, 1-9.

15. Bhullar, K. S.; Rupasinghe, H. *Oxid. Med. Cell. Longev*. **2013**, 1-18.

16. Panda, S.; Chand, M.; Sakhuja, R.; Jain, S. *Curr. Med. Chem*. **2013**, *20* (36), 4481-4507.

17. Rampa, A.; Bisi, A.; Valenti, P.; Recanatini, M.; Cavalli, A.; Andrisano, V.; Cavrini, V.; Fin, L.; Buriani, A.; Giusti P. *J. Med. Chem.* **1998**, *41*, 3976–3986.

18. Belluti, F.; Rampa, A.; Piazzi, L.; Bisi, A.; Gobbi, S.; Bartolini, M.; Andrisano, V.; Cavalli, A.; Recanatini, M.; Valenti, P. *J. Med. Chem.* **2005**, *48*, 4444–4456.

19. Piazzi, L.; Belluti, F.; Bisi, A.; Gobbi, S.; Rizzo, S.; Bartolini, M.; Andrisano, V.; Recanatini, M.; Rampa, A. *Bioorgan. Med. Chem*. **2007**, *15*, 575–585.

20. Qin, J.; Lan, W.; Liu, Z.; Huang, J.; Tang, H.; Wang, H. *Chem. Cent. J*. **2013**, *7* (1), 78.

21. Ramsey, S.; Nguyen, C.; Salomon-Ferrer, R.; Walker, R. C.; Gilson, M. K.; Kurtzman, T. *J. Comp. Chem.* **2016**. *37*, 21, 2029–2037.

22. Nguyen, C. N.; Cruz, A.; Gilson, M. K.; Kurtzman, T. *J. Chem. Theory Comput*. **2014**, *10*, 2769−2780.

23. Ellman, G. L.; Courtney, K. D.; Andres, V.; Featherstone, R. M. A. *Biochem. Pharmacol*. **1961**, *7*, 88-95.

24. Eaton, P. E.; Carlson, G. R.; Lee, J. T. *J. Org. Chem*. **1973**, *38*(23), 4071-4073.

25. Yanga, Z. M.; Huanga, J.; Qina, J. K. Daib, Z. K.; Lana, W. L.; Sua, G. F.; Tanga, H.; Yanga, F. *Eur. J. Med. Chem*. **2014**, *85*, 487-497.

26. Li, R. S.; Wang, X. B.; Hu, X. J.; Kong, L. Y. *Bioorg. Med. Chem. Let*. **2013**, *23*, 2636-2641.

27. Alza, N.P.; Richmond, V.; Baier, C.J.; Freire, E.; Baggio, R.; Murray, A.P. *Bioorg. Med. Chem*. **2014**, *22*, 3838-3849.

28. Perrin, D. D.; Amarego, W. L. F. *Purification of Laboratory Chemicals*, 3rd. ed.,Pergamon Press, Oxford, 1988.

29. Pettersen, E. F.; Goddard, T. D.; Huang, C. C.; Couch, G. S.; Greenblatt, D. M.; Meng E. C.; Ferrin, T. E. *J. Comput Chem.* **2004**, *25* (13), 1605-1612.

30. Morris, G.M; Huey, R; Lindstrom, W; Sanner, M.F; Belew, R.K; Goodsell, D.S; Olson, A.J. *J. Comput. Chem*. **2009**, *16*, 2785-2791.

31. Wallace, A. C.; Laskowski, R. A.; Thornton, J. M. *Protein Eng* **1996**, *8*, 127-134.

32. Laskowski, R. A.; Swindells, M. B. *J. Chem. Inf. Model.* **2011**, *51*, 2778-2786.

33. Case, D. A. et al.**2012**, AMBER 12, University of California, San Francisco.

34. Wang, J., Wang, W., Kollman P. A.; Case, D. A. *J. Mol. Graph. Model* **2006**, *25*, 247- 260.

35. Wang, J., Wolf, R. M.; Caldwell, J. W.; Kollman, P. A.; Case, D. A. *J. Comput. Chem*. **2004**, *25*, 1157-1174.

36. Roe, D. R., Cheatham, T. E. *J. Chem. Theory Comput*. **2013**, *9* (7), 3084–3095.

Graphical abstract

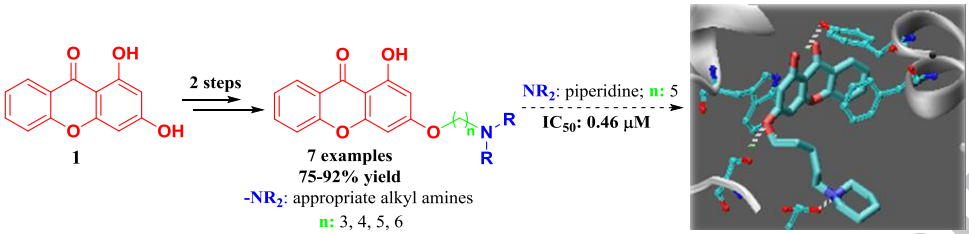

Highlights

- New inhibitors of AChE based on the privileged xanthone scaffold are proposed.
- A rational design of these target structures was conducted.
- A new series of 1,3-dihydroxyxanthone derivatives were easily synthesized.
- The results showed that most of the xanthone derivatives exhibited high AChE.
- Amphiphilic xanthone **11** showed the best inhibitory effect (IC_{50}: 0.46 μM).